

Deep Active Learning for Joint Classification & Segmentation with Weak Annotator

Soufiane Belharbi¹, Ismail Ben Ayed¹, Luke McCaffrey², Eric Granger¹

¹ LIVIA, École de technologie supérieure, Université du Québec, Montreal, Canada

² Rosalind and Morris Goodman Cancer Research Centre, Dept. of Oncology, McGill University, Montreal, Canada

Email: soufiane.belharbi.1@ens.etsmtl.ca, ismail.benayed@etsmtl.ca, luke.mccaffrey@mcgill.ca, eric.granger@etsmtl.ca

ABSTRACT

CNN visualization and interpretation methods, like class activation maps (CAMs), are typically used to highlight the image regions linked to the class predictions. These models allow to simultaneously classify images and yield pixel-wise localization scores, without the need for costly pixel-level annotations. However, they are prone to high false positive localization, and thus poor visualisations when processing challenging images, such as histology images for cancer grading and localization. In this paper, an active learning (AL) framework is proposed to alleviate this issue by progressively integrating pixel-wise annotation during training. Given training data with global class-level labels, our deep weakly-supervised learning (WSL) model simultaneously allows for supervised learning for classification, and active learning for segmentation of images selected for pixel-level annotation by an oracle. Unlike traditional AL methods that focus on acquisition method, we also propose leveraging the unlabeled images to improve model accuracy with less oracle-annotation. To this end, self-learning is considered where the model is used to pseudo-annotate a large number of relevant unlabeled samples, which are then integrated during the learning process with oracle-annotated samples. Our extensive experiments are conducted on complex high resolution medical and natural images from two benchmark datasets – GlaS for colon cancer, and CUB-200-2011 for bird species. Results indicate that by using simply random acquisition, our approach can significantly outperform segmentation obtained with state-of-the-art CAMs and AL methods, using an identical oracle-supervision budget. Our method provides an efficient solution to improve the regions of interest (ROI) segmentation accuracy for real-world visual recognition applications.

1 Introduction

Image classification and segmentation are fundamental tasks in many visual recognition applications involving, e.g., natural and medical images. Given a large image dataset annotated with image-level and pixel-level labels, deep learning (DL) models can be trained end-to-end to achieve state-of-the-art results for these respective tasks (Dolz et al., 2018; Goodfellow et al., 2016; Krizhevsky et al., 2012; Litjens et al., 2017; Long et al., 2015; Ronneberger et al., 2015). However, their impressive accuracy comes at the expense of the considerable cost associated with the collection and annotation of large image datasets for fully supervised learning. While the acquisition of global annotation can be relatively inexpensive, pixel-wise annotation requires a more costly and laborious process. Moreover, in particular application, e.g., medical image analysis, access to domain experts increases the annotation costs.

Code: <https://github.com/sbelharbi/deep-active-learning-for-joint-classification-and-segmentation-with-weak-annotator>

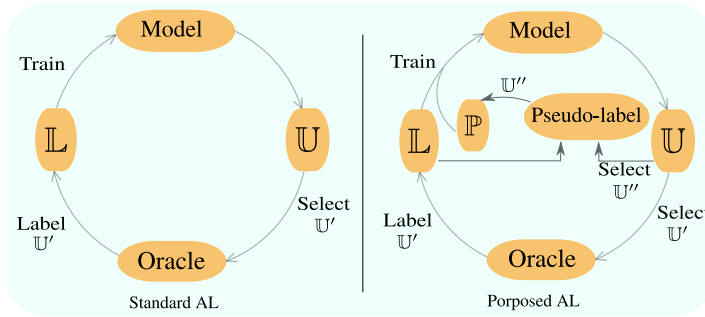


Figure 1: Proposed AL framework with weak annotator.

Weakly-supervised learning (WSL) has recently emerged as a learning paradigm that seeks to limit the need for dense annotation, such as pixel-annotation (Rony et al., 2019; Zhou, 2017). WSL techniques depend on the type of application scenario and annotation, such as global image-level labels (Belharbi et al., 2019b; Kim et al., 2017; Pathak et al., 2015; Teh et al., 2016; Wei et al., 2017), scribbles (Lin et al., 2016; Tang et al., 2018), points (Bearman et al., 2016), bounding boxes (Dai et al., 2015; Khoreva et al., 2017); or global image statistics such as target size (Bateson et al., 2019; Jia et al., 2017; Kervadec et al., 2019a;b). Learning using image-level labels only, which is the focus of this paper, allows to classify an image while yielding pixel-wise scores, thereby localizing the corresponding regions of interest.

Several CNN visualization and interpretation methods have recently proposed, allowing to discover the image regions linked to CNN predictions. In particular, methods based on perturbation, propagation and activation, have been proposed to highlight the regions of an image that are responsible for CNN’s decision. Several WSL techniques (Rony et al., 2019) rely on activation-based methods like CAM, and more recently Gradient-weighted Class Activation Mapping (Grad-CAM), Grad-CAM++, Ablation-CAM, Axiom-based Grad-CAM, etc. (Fu et al., 2020; Lin et al., 2013; Pinheiro and Collobert, 2015). With these methods, a DL model trained using only global annotation can localize the ROIs of the corresponding class in a relatively inexpensive and accurate way. However, while these WSL techniques can provide accurate results in natural images, they cannot accurately localize or segment relatively challenging images, for instance with histology images in medical image analysis (Rony et al., 2019). We note two limitations of CAMs: (1) they are obtained in an unsupervised way (*i.e.* without pixel-level supervision). (2) they have low resolution. For instance, CAMs obtained from ResNet models (He et al., 2016) have a resolution of 1/32 of the input image. Interpolation is required to restore full resolution.

Both of these aspects of CAM-based WSL methods lead to high false positive rates, and therefore, impractical (Rony et al., 2019). Enhancing deep WSL models with pixel-wise annotation is expected to help improve their the localization and segmentation accuracy, which is the central goal of this paper. To do so, we introduce a deep WSL model that allows supervised learning for classification, and active learning for segmentation. The latter is expected to provide more accurate, and high resolution mask for localisation. We assume that images in the training dataset are globally annotated with class-labels. Relevant images are *gradually* labeled at the pixel level through an oracle that respects a low annotation-budget constraint. Consequently, this leads us to active learning (AL) paradigm (Settles, 2009) where an oracle is requested frequently to pixel-wise annotate a subset of selected samples.

Different acquisition techniques have been successfully applied for deep AL for classification based on, e.g., certainty (Ducoffe and Precioso, 2015; Gal et al., 2017; Kirsch et al., 2019) or representativeness (Kim et al., 2020; Sinha et al., 2019) estimation. However, very few deep AL techniques have been proposed for segmentation (Gaur et al., 2016; Górriz Blanch, 2017; Lubrano di Scandalea et al., 2019). Most AL techniques focus mainly on the sampling criterion (Fig.1, left) to populate the supervised pool using an oracle. During training, only the supervised pool is used for training, while the unsupervised pool is left dormant. Such an AL protocol may limit the accuracy

of DL models under constrained oracle-supervision budget in real-world applications for multiple reasons,

(1) standard AL protocol can be practical for small/shallow models that can learn and provide reliable queries using few training samples. Since training accurate DL models is notorious to depend on large number of training samples, large number of queries may be needed to build reliable DL models which results in high annotation cost.

(2) in most AL work, the experimental protocol starts with a large supervised pool; and acquires large size of queries in order to obtain enough supervision neglecting the oracle load. This leads to reach a plateau-performance of a DL quickly hampering a reliable study of the impact of different AL selection techniques. Moreover, model-based sampling techniques are inconsistent (Gaur et al., 2016) since the model is used to query samples while it is still in an early learning stage.

(3) segmentation task shifts some basics of AL compared to classification task such as decision boundaries, and uncertainty which brings additional challenges to AL. For instance, the boundary between classes used in different methods (Ducoffe and Precioso, 2018; Settles, 2009; Tong and Koller, 2001) is not defined for segmentation rendering such branch of methods inadequate for segmentation.

(4) in critical fields such as medical domain, acquiring a sample itself can be very expensive¹. The time and cost associated with each sample makes them valuable items. Such considerations may be overlooked for large scale datasets with almost-free samples such as natural scene images. Due to this high cost, it seems inefficient to keep the unsupervised pool dormant during learning.

Based on the aforementioned arguments, we advocate in this work that: focusing solely on the acquisition function, and relying only on the supervision pool is not an efficient way to build high performing DL models in an AL framework for segmentation task. Therefore, we consider augmenting the supervised pool using the model as second source of annotation in a self-learning fashion (Mao, 2020) (Fig.1, right). This additional annotation can be less accurate (*i.e.* weak²) compared to the oracle that provides strong but expensive annotation. However, it is expected to fast-improve the model's performance (Mao, 2020) while using few oracle-annotated samples cutting the annotation cost.

Our main contributions are: (1) **architecture design**: As an alternative to CAMs, we propose using a segmentation mask trained with pixel annotation and yields more accurate and high resolution segmentation of ROI. This is achieved through a convolutional architecture capable of simultaneously classifying and segmenting images, where the segmentation mask is trained using annotation acquired through AL framework. The architecture is a combination of well known DL models for image classification using ResNet (He et al., 2016) and image segmentation using U-Net (Ronneberger et al., 2015) (Fig.3). Although, different architectures for classification and segmentation could be used as well. (2) **active learning**: To augment the size of the supervised pool by weak-annotating large number of unlabeled samples using the DL model itself, playing the role of a second source of annotation (Fig.1). This allows for rapid improvement of localisation accuracy, with less oracle-based annotation. Moreover, our method can be integrated on top of any acquisition function. (3) **experimental study**: Our experiments are conducted on images from medical and natural scene with high resolution for segmentation – the GlaS dataset for colon cancer using histology images;

¹For instance, prior to a diagnosis of breast cancer from a histological sample, the patient undergoes a bilateral diagnostic mammogram and breast ultrasound that are interpreted by a radiologist, one to several needle biopsies (with low risks under 1% of hematoma and wound infection) to further assess areas of concern, surgical consultation and pre-operative blood work, and surgical excision of tissue positive for breast cancer cells. The biopsy and surgical tissues are processed (fixation, embedding in paraffin, H&E staining) and interpretation by a pathologist. Depending on the cancer stage, the patient may undergo additional procedures. Therefore, when accounting for all steps required for breast cancer diagnosis from histological samples, a rough estimation of the final cost associated with obtaining a Whole Slide Image (WSI) is about \$400 (Canadian dollars, by 1999) (Will et al., 1999). Moreover, some cancer types are rare (Will et al., 1999), making these samples even more valuable. All these procedures are conducted by highly trained experts where each procedure may take few minutes to an hour, and require expensive specialized medical equipment.

²To not be confused with weak annotation in weakly supervised learning framework.

and CUB-200-2011 dataset for bird species. The experiments are achieved using a realistic AL protocol that takes into consideration the annotator’s effort by minimizing the number of queries that in a real-application. Such protocol allows a better study of the different acquisition functions. To demonstrate the efficiency of our method, we simply use random sampling.

2 Related work

Deep active learning. AL has been studied for long time in machine learning mainly for classification and regression, using linear models in particular (Settles, 2009). Recently, there has been an effort to transfer such techniques to DL models for classification task by mimicking their intuition or adapting them based on DL models’ specificities and taking in consideration their complexity. Such methods include for instance, different mechanisms for uncertainty (Beluch et al., 2018; Ducoffe and Precioso, 2015; 2018; Gal et al., 2017; Kim et al., 2020; Kirsch et al., 2019; Lakshminarayanan et al., 2017; Wang et al., 2016; Yoo and Kweon, 2019), and representativeness (Kim et al., 2020; Sener and Savarese, 2018; Sinha et al., 2019) estimation. Although, most deep AL techniques are validated on synthetic, simple, or tiny data rather than real data which does not explore their full potential in real applications.

While deep AL for classification is rapidly emerging, deep AL for segmentation grows with slow rate leading to very sparse literature. In fact, the very few proposed methods are a direct application of deep AL methods for classification with few exceptions. This slow rate in research may be explained by the fact that segmentation task brings additional challenges to AL including the spatial information of the segmentation mask that lies in large dimension. In classification, AL often deals with one output that is used as the core that drives queries (Huang et al., 2010). The spatial information in segmentation does not provide naturally a direct scoring function that can indicate the overall quality or certainty of the output. Most of deep AL methods for segmentation consider pixels as classification instances, then a standard AL technique for classification is applied at each pixel. The final score of the sample is the average score at pixel-level.

For instance, the authors of (Gaur et al., 2016) simply exploit a variant of entropy-based acquisition at pixel-level, combined with a distribution-based term that encodes diversity using a complex hierarchical clustering algorithm over sliding windows with an application to microscopic membrane segmentation. Similarly, (Górriz Blanch, 2017; Lubrano di Scandalea et al., 2019) apply Monte-Carlo dropout uncertainty (Gal et al., 2017) at pixel-level with application to myelin segmentation using spinal cord and brain microscopic histology images. In (Roels and Saeys, 2019), the authors experiment with five acquisition function of classification for a segmentation task including entropy-based, core-set (Sener and Savarese, 2018), k-mean, and Bayesian (Gal et al., 2017) sampling with application to electron microscopy segmentation. Entropy-based methods seem to be dominant over multiple datasets. In (Yang et al., 2017), the authors combine two sampling terms for histology image segmentation. The first employs bootstrapping over fully convolutional networks (FCN) to estimate uncertainty where a set of FCNs are trained on different subsets of samples. The second term is a representation-based term that selects the most representative samples. This is achieved by solving an optimization of a generalization version of the maximum cover set problem (Feige, 1998) using sample description extracted from an FCN. Despite the obtained promising results, this approach remains complex and impractical due to the use of bootstrapping over DL models and an optimization step. Moreover, the authors of (Yang et al., 2017) do not provide a comparison to other acquisition functions. The work in (Casanova et al., 2020) considers a specific case of AL using reinforcement learning for *region-based* AL for segmentation where only a selected region of the image is labeled in the opposite to the entire image in standard AL. This method is adequate for datasets with large and unbalanced classes such as street view images. While the proposed method in (Casanova et al., 2020) outperforms random, and Bayesian (Gal et al., 2017) selection, surprisingly it performs close to entropy-based selection.

Weak annotators. AL paradigm does not prohibit the usage of the unsupervised pool for training (Settles, 2009), but it mainly constrains the oracle-labeling budget. AL standard experimental protocol (Fig.1, left) was inherited from AL of simple/linear models and passed to subsequent works. To build robust DL models, oracle-based annotation may be insufficient due to the lack of

supervision. Leveraging furthermore the unsupervised pool for more supervision has been seen in AL for classification (Long et al., 2008; Vijayanarasimhan and Grauman, 2012; Wang et al., 2016; Zhou et al., 2010; Zhu et al., 2003).

For instance, the authors of (Wang et al., 2016) propose to pseudo-label part of the unlabeled pool, selected using dynamic thresholding based on confidence, through the model itself to learn better embedding. Furthermore, a theoretical framework for AL using strong and weak annotators for classification task is introduced in (Zhang and Chaudhuri, 2015). The obtained results suggest that using multiple annotators can bring savings to oracle expensive annotation compared to one annotator. Using multiple source of annotation that include strong and weak annotators has been used in AL, crowd-sourcing, self-paced learning and other interactive learning scenarios for classification to help reducing the number of requests for the strong annotator (Kremer et al., 2018; Malago et al., 2014; Mattsson, 2017; Murugesan and Carbonell, 2017; Urner et al., 2012; Yan et al., 2016; Zhang and Chaudhuri, 2015), which in turn helps reducing a major part of the annotation cost. Using the model itself for pseudo-annotation is motivated mainly by the success of self-supervised learning in DL (Mao, 2020).

Label propagation (LP). Our proposed approach is also related to LP methods (Bengio et al., 2010; Zhou et al., 2004; Zhu and Ghahramani, 2002) for classification since they both aim to label unlabeled samples using knowledge from supervised samples (Fig.2). However, while LP propagates labels to unlabeled samples through an iterative process, our approach bypasses this using the model itself; and the propagation is limited to the neighbors of labeled samples defined through k -nearest neighbors (k -nn) (Fig.2). Using k -nn has been also studied to combine AL and domain adaptation (Berlind and Urner, 2015) where the goal is to query samples from the target domain in a way that all the labeled samples form a coverset for the leftover unlabeled set in order to build an accurate k -nn classifier. Such approach is connected to the recently developed core-set method for deep AL (Sener and Savarese, 2018). Our method intersects with (Berlind and Urner, 2015) only in the sense of using a label prediction procedure involving labeled neighbors to query samples. In our case, labeled samples are used as landmarks to acquire more unlabeled samples for pseudo-annotation.

Different from state of the art of deep AL methods for segmentation, we consider increasing the supervised pool through weakly annotated samples (Fig.1, right). To this end, the model is used for pseudo-labeling samples located in the neighborhood of samples with strong supervision (Fig.2). From self-learning perspective, the work in (Wang et al., 2016) is the closest to ours where they include samples with high confidence to the supervised pool. Our pseudo-labeled samples are added to the supervised pool along with the samples annotated by the oracle and used for training. The underlying assumption is that given a sample labeled by an oracle, the model is more likely to produce good segmentation of images located nearby that sample. Our assumption is empirically verified later in the experimental section. This simple procedure allows to quickly increase the number of pseudo-labeled samples to help fast-improve the model’s performance for segmentation under a limited oracle-based supervision.

3 Proposed approach

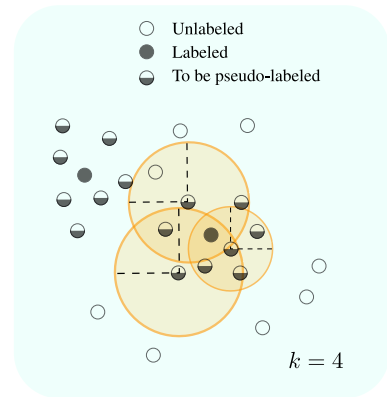


Figure 2: The k -nn method for selecting \mathbb{U}'' subset to be pseudo-labeled. Assumption to select \mathbb{U}'' : since \mathbb{U}'' lives nearby supervised samples, it is more likely to be assigned good segmentation by the model. We consider measuring k -nn for each **unlabeled** sample. In this example, using $k = 4$ allows $|\mathbb{U}''| = 14$. If k -nn is considered for each **labeled** sample: $|\mathbb{U}''| = 8$. $|\cdot|$ is the set cardinal. Note: k -nn is considered *only* between samples of the *same class*.

We consider an active learning problem for weakly supervised segmentation where all training images have class-level annotation, but no pixel-level annotations. Due to the high cost of pixel-annotation, they are gradually acquired from an oracle through queries.

Active learning training consists of sequential training rounds. At each round r , the total trainset \mathbb{D} that contains n samples is composed of unlabeled, and labeled subsets (Fig.1). **(1) Unlabeled subset:** contains samples without pixel-wise annotation (unlabeled samples) $\mathbb{U} = \{\mathbf{x}_i, y_i, -\}_{i=1}^u$ where $\mathbf{x} \in \mathcal{X}$ is the input image, y is its global label; and the pixel label is missing. **(2) Labeled subset:** contains samples with full supervision $\mathbb{L} = \{\mathbf{x}_i, y_i, \mathbf{m}_i\}_{i=1}^l$ where \mathbf{m} is the pixel-wise annotation of the sample. \mathbb{L} is initially empty. It is replenished gradually from \mathbb{U} by querying the oracle using an acquisition function. $f(\cdot : \theta)$ is a DL model that is able to classify and segment an image \mathbf{x} (Fig.3). For clarity, and since we focus on the segmentation task, we neglect the notation for classification task. Therefore, $f(\mathbf{x})$ refers to the predicted segmentation mask. We note $\mathbb{U}' \subseteq \mathbb{U}$, $\mathbb{U}'' \subseteq \mathbb{U}$ two subsets (Fig.1) where $\mathbb{U}' \cap \mathbb{U}'' = \emptyset$. In our method, we introduce \mathbb{P} as a subset holder for pseudo-labeled samples. It is initially empty, and it is replenished gradually (Fig.1, right). To express the dependency of each subset with respect to a round r , we note $\mathbb{U}_r, \mathbb{L}_r, \mathbb{P}_r, \mathbb{U}'_r, \mathbb{U}''_r$. Samples in \mathbb{P}_r are noted $\{\mathbf{x}_i, y_i, \hat{\mathbf{m}}_i\}$. This holds: $\forall r : \mathbb{D} = \mathbb{L}_r \cup \mathbb{U}_r \cup \mathbb{P}_r$.

Alg.1 describes the overall active learning process and our pseudo-annotation method. First, \mathbb{U}'_r is queried, then labeled by the oracle, and added to \mathbb{L}_r . Using k -nn, \mathbb{U}''_r is selected based on their proximity to \mathbb{L}_r (Fig.2); and pseudo-labeled by the model, then added to \mathbb{P}_r . To fast-increase the size of \mathbb{L}_r , \mathbb{P}_r is protected from being queried for the oracle until it is inevitable. In the *latter case*, queried samples from \mathbb{P}_r are used to fill \mathbb{U}' ; and they are no longer considered pseudo-labeled since they will be assigned the oracle annotation.

To measure images similarity for k -nn method, color distribution is used to describe an image content which can be a flexible descriptor for highly unstructured images such as histology images. Note that k -nn method is considered *only* between samples of the *same class*. The underlying assumption is that samples of the same class with similar color distribution are likely to contain relatively similar objects with related texture. Consequentially, labeling one sample of them can allow the model to access to supervised learning of such distribution. This can increase the likelihood of the model to provide relatively good segmentation of the other samples. The proximity between two images $(\mathbf{x}_i, \mathbf{x}_j)$ is measured using Jensen-Shannon divergence between their respective histogram color distribution. For an image with multiple color planes, the similarity is formulated as the sum of similarity of each plane.

At round r , the queried and the pseudo-labeled samples are both used in training by optimizing the following equation,

$$\min_{\theta} \sum_{\mathbf{x}_i \in \mathbb{L}_{r-1}} \mathcal{L}(f(\mathbf{x}_i), \mathbf{m}_i) + \lambda \sum_{\mathbf{x}_i \in \mathbb{P}_{r-1}} \mathcal{L}(f(\mathbf{x}_i), \hat{\mathbf{m}}_i), \quad (1)$$

where $\mathcal{L}(\cdot, \cdot)$ is a segmentation loss, λ is a positive scalar. Eq.1 trains the model (Fig.3) solely for segmentation task. Simultaneous training of the model for classification and segmentation tasks in this AL setup is avoided due to the unbalance between the number of samples labeled globally and at pixel-level. Therefore, we consider training the model for classification first, then freeze the classifier

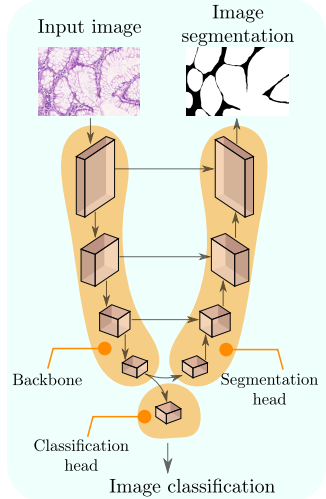


Figure 3: Hybrid architecture for classification and segmentation with U-Net style (Ronneberger et al., 2015) composed of: (1) a shared **backbone** for feature extraction; (2) **classification head** for classification task; (3) and **segmentation head** for segmentation task. The latter merges representations from the backbone while upscaling the feature maps gradually to reach the full image resolution for the predicted mask similarly to U-Net model.

parameters. Training for segmentation tasks is resumed later. This yields the best classification performance, and it allows a better study of the impact of the queried samples on segmentation task.

Algorithm 1: Standard AL procedure and our proposal.
 Extra instructions associated only with our method are indicated with a blue background. Line-10 pseudo-labels the entire \mathbb{P}_r at each round to update the pseudo-masks since the model is expected to improve which in turn improves the pseudo-segmentation.

| | |
|----------------|--|
| Input : | $\mathbb{P}_0 = \mathbb{L}_0 = \emptyset$ |
| | θ^0 : initial parameters of f trained on classification task. |
| | maxr : maximum number of AL rounds. |
| 1 | Select \mathbb{U}'_0 randomly and label them by an oracle. |
| 2 | $\mathbb{L}_0 \leftarrow \mathbb{U}'_0$. |
| 3 | for $r \in 1 \cdots \text{maxr}$ do |
| 4 | $\theta \leftarrow \theta^0$. |
| 5 | Train f using $\mathbb{L}_{r-1} \cup \mathbb{P}_{r-1}$ using Eq.1. |
| 6 | Select \mathbb{U}'_r and label them by an oracle. |
| 7 | $\mathbb{L}_r \leftarrow \mathbb{L}_{r-1} \cup \mathbb{U}'_r$. |
| 8 | Select \mathbb{U}''_r . |
| 9 | $\mathbb{P}_r \leftarrow \mathbb{P}_{r-1} \cup \mathbb{U}''_r$. |
| 10 | Pseudo-label \mathbb{P}_r . |

4 Results and discussion

4.1 Experimental methodology:

a) Datasets. For evaluation, datasets should have global and pixel-wise annotation. We consider two public datasets in medical and natural scene with real and high resolution images (Fig.4). (1) **GlaS dataset**: a histology images dataset for colon cancer diagnosis³ (Sirinukunwattana et al., 2017). It is composed of 165 images derived from 16 Hematoxylin and Eosin (H&E) histology sections of two grades (classes): benign, and malignant. It is divided into 84 samples for training, and 80 samples for test. The ROI required to be segmented are the glandes. (2) **CUB-200-2011 dataset (CUB)**⁴ (Wah et al., 2011) is a dataset for bird species with 11,788 samples (5,994 for train and 5,794 for test) and 200 species. The ROI required to be segmented are the birds. In GlaS, and CUB datasets, we randomly select 80% of training samples for effective training, and 20% for validation (with full supervision) to perform early stopping. The splits are similar to the ones used in (Belharbi et al., 2019a; Rony et al., 2019); and they are publicly available.

³GlaS: warwick.ac.uk/fac/sci/dcs/research/tia/glascontest.

⁴CUB: www.vision.caltech.edu/visipedia/CUB-200-2011.html

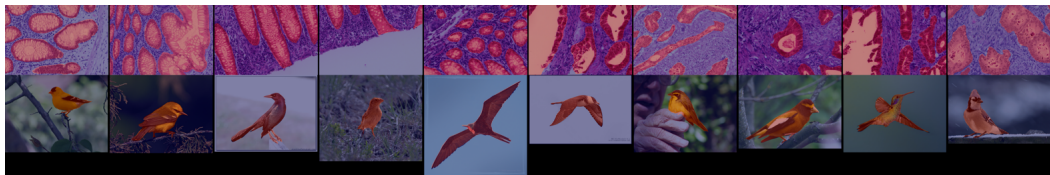


Figure 4: **Top row:** GlaS dataset (Sirinukunwattana et al., 2017). **Bottom row:** CUB dataset (Wah et al., 2011). (Best visualized in color.)

Table 1: Number of samples selected for the oracle per round.

| Dataset | #selected samples <i>per-class</i> ($r = 1$) | #selected samples <i>per-class</i> ($r > 1$) | Max AL rounds ($\max r$ in Alg.1) |
|---------|---|---|---------------------------------------|
| GlaS | 4 | 1 | 25 |
| CUB | 1 | 1 | 20 |

b) Active learning setup. To assess the performance of different AL acquisition methods, we consider a realistic scenario with respect to the number of samples to be labeled at each AL round to take into account the load on the oracle. Therefore, only few samples are selected at each round for oracle-annotation, and \mathbb{L} is slowly replenished. This allows better comparison between AL selection techniques since we spend more time in a phase where \mathbb{L} holds few samples. Such phase allows to better measure the impact of the selected samples. Filling \mathbb{L} quickly brings the model’s performance to a plateau that hides the impact a newly selected samples. The initial replenishment ($r = 1$) is achieved by randomly selecting few samples. The same samples are used for all AL techniques at round $r = 1$ for a fair comparison. To avoid any bias from selecting unbalanced classes that can directly affect the segmentation performance, and hinder AL evaluation, the same number of samples is selected from each class since the global annotation is known beforehand for all samples. Note that the oracle is only required to provide pixel-wise annotation. Tab.1 provides the selection details.

c) Evaluation. We report the classification accuracy obtained by the classification head (Fig.3). Average Dice index is used to measure the segmentation quality at each AL round forming a Dice index curve over all the rounds. To better assess the *dominance* of each method (Settles, 2009), the Area Under the Dice index Curve is used (AUC). This provides a fair indicator of the dominant curve, but contrasts with standard AL work where the authors select one or multiple specific operating points in the curve (leading to a biased and less accurate protocol). The average and the standard deviation of Dice index curve and AUC metric are reported based on 5 replications of a complete AL session, using different seed for each session. An AL session across different methods uses the same seed.

While our approach, referred to as (Label_prop), can operate on top of any AL selection criterion, we demonstrate its efficiency using random selection which is often a baseline for AL experiments. It is compared to three different AL selection approaches for segmentation: (1) **random selection (Random)** where samples are randomly selected. (2) **entropy-based selection (Entropy)**: the scoring function per sample is the average entropy at pixel level (Gaur et al., 2016). Samples with high entropy are selected. (3) **Monte-Carlo dropout uncertainty (MC_Dropout)**: we use Monte-Carlo dropout (Górriz Blanch, 2017; Lubrano di Scandalea et al., 2019) at pixel-level to compute the uncertainty score per sample. Samples are forwarded 50 times in the model where dropout is set to 0.2 (Górriz Blanch, 2017; Lubrano di Scandalea et al., 2019). Then, the pixel-wise variance is estimated. Samples with high mean variance are selected.

Lower bound performance (WSL). We consider the segmentation performance obtained by WSL method as a lower bound. It is trained using only global annotation. CAMs are used to extract the segmentation mask. WILDCAT method is considered (Durand et al., 2017) (Fig.3) at the classification head to obtain the CAMs. For WSL method, a pre-trained model over ImageNet (Deng et al., 2009) is used to initialize the weights of the backbone which is then fine-tuned. The model is trained over the entire dataset where samples are labeled globally only. The obtained classifier using seed=0 is frozen and used as a backbone for *all* the other methods.

Upper bound performance (Full_sup). Full supervised segmentation is considered as an upper bound performance. The model in Fig.3 is trained for segmentation only using the entire dataset where samples are labeled at pixel-level.

For a fair comparison, all methods are trained using the same hyper-parameters over the same dataset. WSL and Full_sup methods have minor differences. Due to space limitation, all the hyper-parameters are presented in the supplementary material. In Alg.1, notice that for our method, \mathbb{P}_r is not used at the current round r but until the next round $r + 1$. To take advantage of \mathbb{P}_r at round r , instructions from line-4 to line-10 are repeated twice in the provided results.

Table 2: Classification accuracy over of the proposed deep WSL model on GlaS and CUB test datasets.

| Dataset | GlaS | CUB |
|-----------------------------|------------------|------------------|
| Classification accuracy (%) | 99.50 ± 0.61 | 73.22 ± 0.19 |

4.2 Results

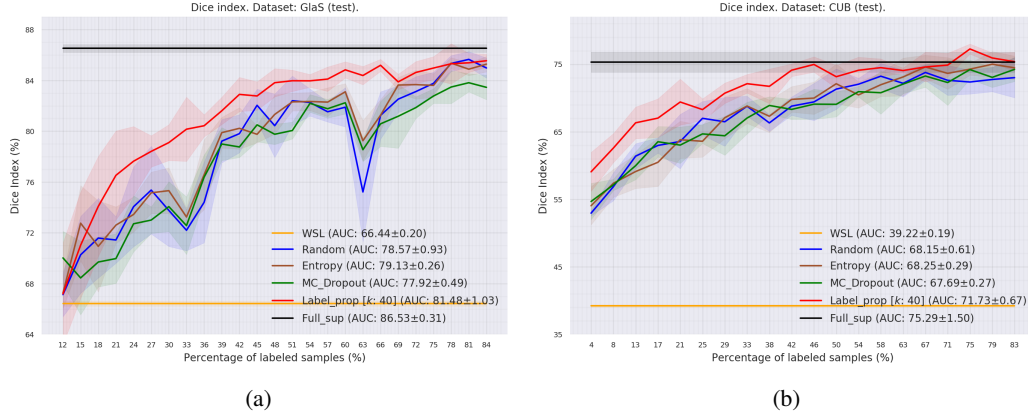


Figure 5: Average Dice index of the proposed and baseline methods over test sets. (a) GlaS. (b) CUB.

Table 3: Average AUC and standard deviation (Fig.5) for Dice index performance over GlaS and CUB test sets.

| Dataset | GlaS | CUB |
|--------------------------|------------------------------------|------------------------------------|
| WSL | 66.44 ± 0.20 | 39.22 ± 0.19 |
| Random | 78.57 ± 0.93 | 68.15 ± 0.61 |
| Entropy | 79.13 ± 0.26 | 68.25 ± 0.29 |
| MC_Dropout | 77.92 ± 0.49 | 67.69 ± 0.27 |
| Label_prop (ours) | 81.48 ± 1.03 | 71.73 ± 0.67 |
| Full_sup | 86.53 ± 0.31 | 75.29 ± 1.50 |

After training the proposed deep WSL model in Fig.3, classification and segmentation performance are reported. Classification accuracy of the classification head using WSL is reported in Tab.2 which are close to the results reported in (Belharbi et al., 2019b; Rony et al., 2019). The results of GlaS suggest that it is an easy dataset for classification.

Segmentation results are reported in Tab.3,4, and Fig.5. Fig.5a compares Dice accuracy on the **GlaS dataset** on which we can observe that adding more labels increases Dice index for all AL methods allowing better performance than WSL method as expected. Reading from Tab.4, randomly labeling only 4 samples per class allows to easily outperform WSL. This means that using our approach in Fig.3 with limited supervision can lead to more accurate masks compared to using CAMs in WSL method. From Fig.5a, one can also observe that Random, Entropy, and MC_Dropout methods grow relatively in the same way leading to the same overall performance where Entropy method is slightly ahead. Considering the overall behavior of the curves, one may conclude that using advanced selection techniques such as MC_Dropout, and Entropy provides a similar accuracy to simple random

Table 4: Readings of Dice index (mean \pm standard deviation) from Fig.5 over test set for the **first 5 queries** formed by each method. We start from the second query since the first query is random but identical for all methods.

| Queries | q2 | q3 | q4 | q5 | q6 |
|--------------------------|------------------------------------|------------------------------------|------------------------------------|------------------------------------|------------------------------------|
| GlaS | | | | | |
| WSL | 66.44 ± 0.20 | | | | |
| Random | 70.26 ± 3.02 | 71.58 ± 3.14 | 71.43 ± 1.83 | 74.05 ± 3.14 | 75.36 ± 3.45 |
| Entropy | 72.75 ± 2.96 | 70.93 ± 3.58 | 72.60 ± 1.44 | 73.44 ± 1.38 | 75.15 ± 1.63 |
| MC_Dropout | 68.44 ± 2.89 | 69.70 ± 1.96 | 69.97 ± 1.95 | 72.71 ± 2.21 | 73.00 ± 1.04 |
| Label_prop (ours) | 71.02 ± 4.19 | 74.07 ± 3.93 | 76.52 ± 3.49 | 77.63 ± 2.73 | 78.41 ± 1.23 |
| Full_sup | 86.53 ± 0.31 | | | | |
| CUB | | | | | |
| WSL | 39.22 ± 0.18 | | | | |
| Random | 56.86 ± 2.07 | 61.39 ± 1.85 | 62.97 ± 1.13 | 63.56 ± 4.02 | 66.56 ± 2.50 |
| Entropy | 53.37 ± 2.06 | 59.11 ± 2.50 | 60.48 ± 3.56 | 63.81 ± 2.75 | 63.59 ± 2.34 |
| MC_Dropout | 57.13 ± 0.83 | 59.98 ± 2.06 | 63.52 ± 2.26 | 63.02 ± 2.68 | 64.68 ± 1.41 |
| Label_prop (ours) | 62.58 ± 2.15 | 66.32 ± 2.34 | 67.01 ± 2.85 | 69.40 ± 3.40 | 68.28 ± 1.60 |
| Full_sup | 75.29 ± 1.50 | | | | |

selection. Since both methods have shown substantial improvements in AL for classification, and based on the results in Fig.5a, we can understand that the potential reason behind such results is that all samples are equivalently informative for the model. Therefore, there is no better order to acquire them. On the other hand, using simply random selection and pseudo-labeled samples allowed our method to substantially improve the overall performance demonstrating the benefits of self-learning.

Fig.5b, and Tab.4 compare Dice accuracy on the **CUB dataset**, where labeling only one sample per class allows a large improvement in Dice index compared to WSL. Adding more samples increases the performance of all the methods. One can observe similar pattern as for GlaS where Random, Entropy, and MC_Dropout methods yield similar curves where Random and Entropy methods obtain similar AUC performance slightly ahead of MC_Dropout. Similar to GlaS analysis, and based on the results of these three methods, one can conclude that there is no efficient way to order the samples for annotation in order to obtain higher performance than simple random selection. Using self-labeled samples in our method shows again its benefits. Simple random selection combined with self-annotation yields an overall better and consistent performance. Using two datasets, our empirical results suggest that self-learning, under limited oracle-annotation, has the potential to provide a reliable second source of annotation that can efficiently enhance model performance while using simple sample acquisition techniques.

Pseudo-annotation performance. Furthermore, the proposed approach is assessed on the pseudo-labeled samples at each AL round. Fig.6 shows that the model provides good segmentation from the initial rounds. Then, the further we add supervision the more the pseudo-segmentation is accurate as expected. This figure shows the interest and potential of self-learning in segmentation, and confirms our assumption that samples near labeled ones are likely to achieve accurate pseudo-segmentation by the model.

Hyper-parameters. Our approach requires two main hyper-parameters: k and λ . We conducted an ablation study over k on GlaS dataset, and over λ on both datasets. Results are presented in the supplementary material. The results suggest that our method is less sensitive to k . In other hand, λ plays an important role which is known to be the case in penalty-based optimization methods as in Eq.1 (Bertsekas, 1999). Based on our study, we recommend using small values of λ . In our experiments, we used fixed values for $\lambda = 0.1, 0.001$ for GlaS and CUB, respectively. We set $k = 40$. Although, hyper-parameters tuning in AL is challenging due to the change of the size of data which in turn changes the training dynamic. In all the experiments, we used fixed hyper-parameters across

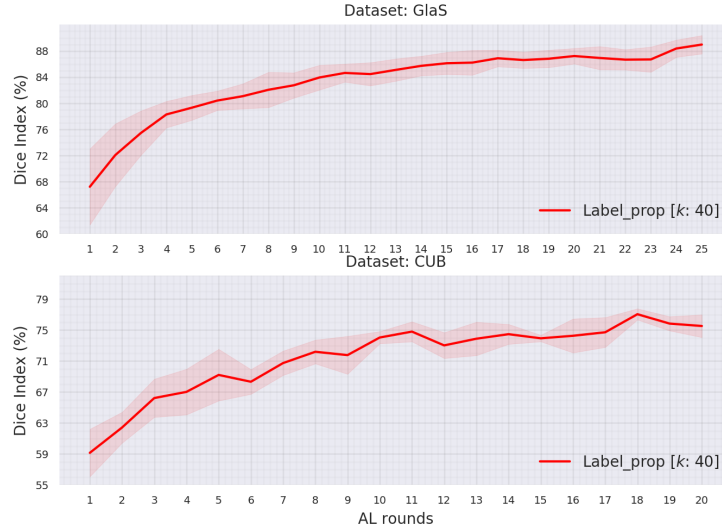


Figure 6: Average Dice index over the pseudo-labeled samples of our method in **each** AL round.

the AL rounds. Fig.6 suggests that a dynamic $\lambda(r)$ that is increased through AL rounds could be more beneficial. However, this requires a principled update protocol for λ which was not explored in this work. Nonetheless, using a fixed value seems to yield promising results overall.

Supplementary material. Due to space limitation, we provide in the supplementary material detailed hyper-parameters used in the experiments, results of the ablation study, visual results to the similarity measure, and examples of predicted masks.

5 Conclusion

CAMs of WSL methods, often obtained using global annotation, play an important role in CNN visualization and interpretability. However, they are prone to high false positive especially for challenging images leading to poor segmentation of ROI. To alleviate this issue, we considered using pixel-wise supervision provided gradually through an AL framework. This annotation is integrated into training using an adequate deep convolutional model that allows supervised learning of both tasks: classification, and segmentation. Through few pixel-supervised samples, such design is intended to provide full resolution and more accurate masks compared to standard CAMs that are trained without pixel-supervision, and often have low resolution. Therefore, a better visualization of ROI can be achieved. Furthermore, and unlike standard deep AL methods that focus solely on the acquisition function, we considered using self-learning as a second source of supervision to fast-improve the model segmentation. Evaluated using realistic AL protocol over two benchmarks, our results showed that: (1) using *few* supervised samples, the proposed architecture allowed obtaining more accurate segmentation compared to CAMs with large margin using different AL methods. Thus, it provides an efficient solution to improve the regions of interest (ROI) segmentation accuracy for real-world visual recognition applications. (2) using self-learning with random selection allowed substantial improvements. This could make self-learning under limited oracle-budget a better alternative to standard AL protocol where most of the effort is spent on the acquisition function.

Acknowledgment

This research was supported in part by the Natural Sciences and Engineering Research Council of Canada, MITACS, and the Ericsson Global AI Accelerator Montreal.

A Supplementary material for the experiments

Due to space limitation, we provide in this supplementary material detailed hyper-parameters used in the experiments, results of the ablation study, visual results to the similarity measure, and examples of predicted masks.

A.1 Training hyper-parameters

Tab.5 shows the used hyper-parameters in all our experiments.

Table 5: Training hyper-parameters.

| Hyper-parameter | GlaS | CUB |
|--------------------------------|-----------------------------|-----------------------|
| Model backbone | ResNet-18 (He et al., 2016) | |
| WILDCAT (Durand et al., 2017): | | |
| α | 0.6 | |
| k_{min} | 0.1 | |
| k_{max} | 0.1 | |
| modalities | 5 | |
| Optimizer | SGD | |
| Nesterov acceleration | True | |
| Momentum | 0.9 | |
| Weight decay | 0.0001 | |
| Learning rate (LR) | 0.1 (WSL: 10^{-4}) | 0.1 (WSL: 10^{-2}) |
| LR decay | 0.9 | 0.95 (WSL: 0.9) |
| LR frequency decay | 100 epochs | 10 epochs |
| Mini-batch size | 20 | 8 |
| Learning epochs | 1000 | 30 (WSL: 90) |
| Horizontal random flip | True | |
| Vertical random flip | True | False |
| Crop size | 416×416 | |
| k | 40 | |
| λ | 0.1 | 0.001 |

A.2 Ablation study

We study the impact of k and λ on our method. Results are presented in Fig.7, 8 for GlaS over k, λ ; and in Fig.9 for CUB over λ . Due to the expensive computation time required to perform AL experiments, we limited the experiments (k, λ , number of trials, and `maxr`). The obtained results of this study show that our method is less sensitive to k (standard deviation of 0.59 in Fig.7). In other hand, the method shows sensitivity to λ as expected from penalty-based methods (Bertsekas, 1999). The obtained results recommend using small values that lead to better and stable performance. Using high values, combined with the pseudo-annotation errors, push the network to learn erroneous annotation leading to overall poor performance.

A.3 Similarity measure

In this section, we present some samples with their nearest neighbors. Although, it is difficult to quantitatively evaluate the quality of such measure. Fig.10 shows the case of GlaS. Overall, the similarity shows good behavior of capturing the general stain of the image which is what was intended for since the structure of such histology images is subject to high variation. Since the stain variation

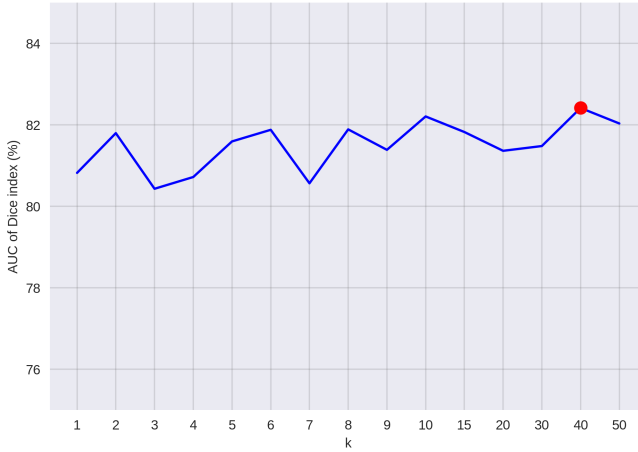


Figure 7: Ablation study over GlaS dataset (test set) over the hyper-parameter k (x-axis). y-axis: AUC of Dice index (%) of **25 queries for one trial**. AUC average \pm standard deviation: 81.49 ± 0.59 . Best performance in red dot: $k = 40$, $AUC = 82.41\%$.

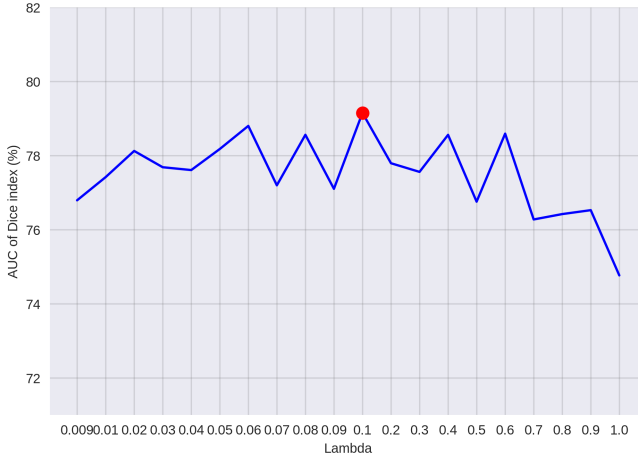


Figure 8: Ablation study over GlaS dataset (test set) over the hyper-parameter λ (x-axis). y-axis: AUC of Dice index (%) of **15 queries for one trial**. Best performance in red dot: $\lambda = 0.1$, $AUC = 79.15\%$.

is one of the challenging aspects in histology images (Rony et al., 2019), labeling a sample with a common stain can help the model in segmenting other samples with similar stain. The case of CUB, presented in Fig.11, is more difficult to judge the quality since the images contain always the same species within their natural habitat. Often, the similarity succeeds to capture the overall color, background which can help segmenting the object in the neighbors and also the background. In some cases, the similarity captures samples with large zoom-in where the bird color dominate the image.

A.4 Predicted mask visualization

Fig.12 shows several test examples of predicted masks of different methods over CUB test set at the first AL round ($r = 1$) where only one sample per class has been labeled by the oracle. This interesting functioning point shows that by labeling only one sample per class, the performance of the average Dice index can go from 39.08 ± 08 for WSL method up to 62.58 ± 2.15 for Label_prop and other AL methods. The figure shows that WSL tend to spot small part of the object in addition to the background leading high false positive. Using few supervision in combination with the proposed

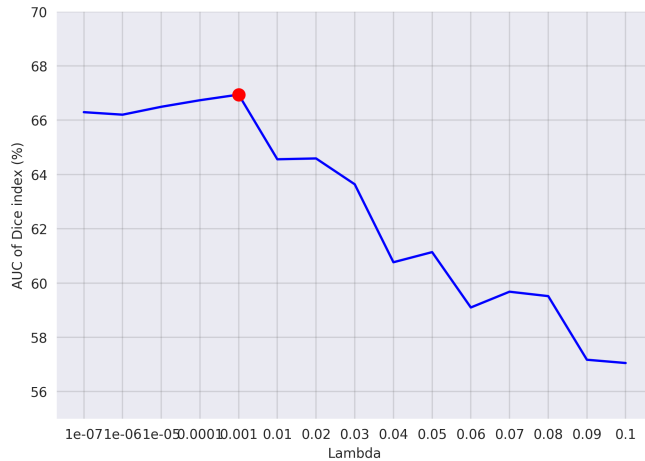


Figure 9: Ablation study over CUB dataset (test set) over the hyper-parameter λ (x-axis). y-axis: AUC of Dice index (%) of **5 queries for one trial**. Best performance in red dot: $\lambda = 0.001$, $AUC = 66.94\%$.

architecture, better segmentation is achieved by spotting large part of the object with less confusion with the background.

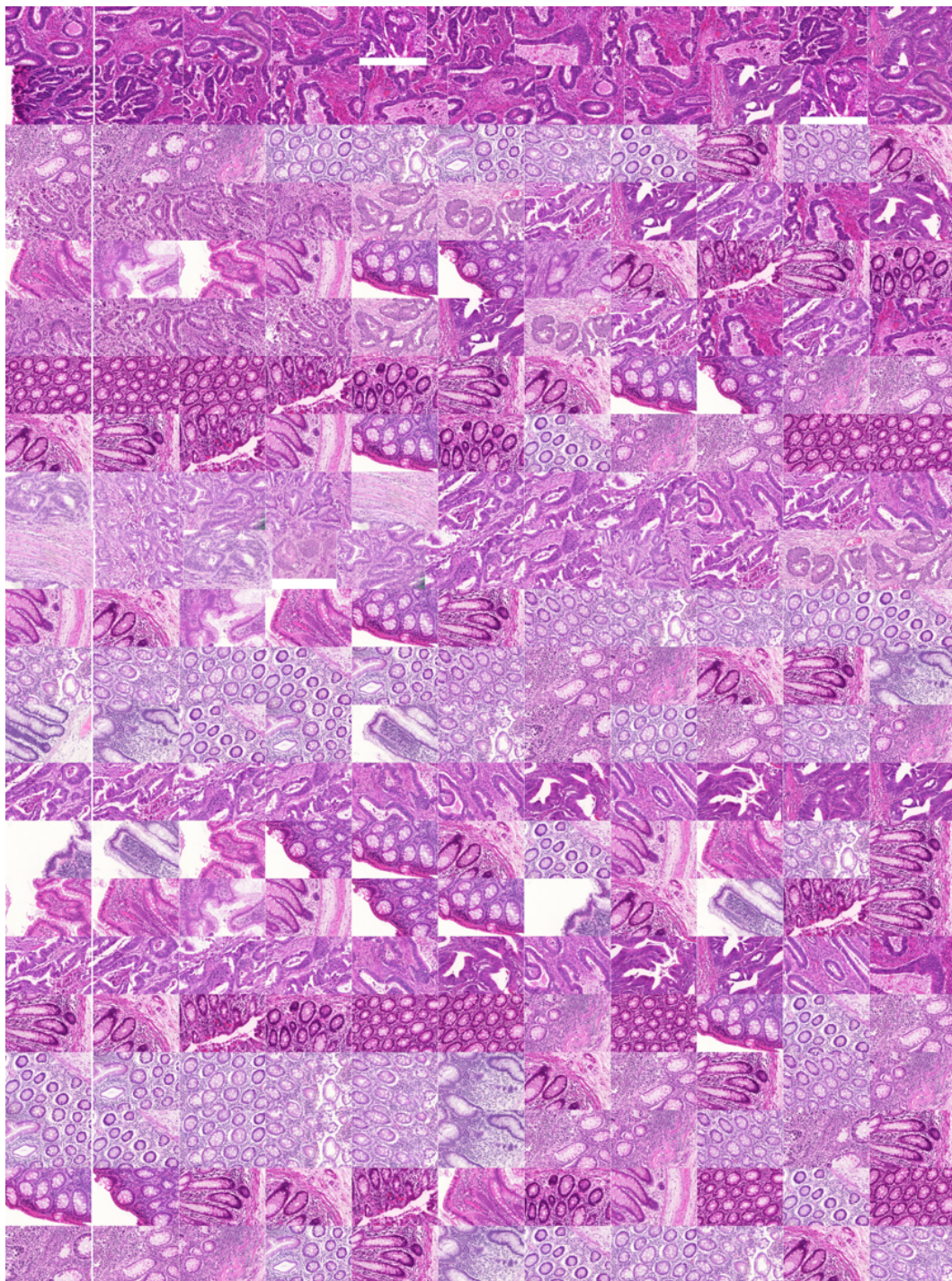


Figure 10: Examples of k -nn over GlaS dataset. The images represents the 10 nearest images to the first image in the extreme left ordered from the nearest.



Figure 11: Examples of k -nn over CUB dataset. The images represents the 10 nearest images to the first image in the extreme left ordered from the nearest.



Figure 12: Qualitative results (on several CUB test images) of the predicted binary mask for each method after being trained in the first round $r = 1$ (i.e. after labeling 1 sample per class) using seed=0. The average Dice index over the test set of each method is: 40.16% (WSL), 55.32% (Random), 55.41% (Entropy), 55.52% (MC_Dropout), 59.00% (Label_prop), and 75.29% (Full_sup). (Best visualized in color.)

References

Bateson, M., Kervadec, H., Dolz, J., Lombaert, H., and Ben Ayed, I. (2019). Constrained domain adaptation for segmentation. In *MICCAI*.

Bearman, A., Russakovsky, O., Ferrari, V., and Li, F. (2016). What's the point: Semantic segmentation with point supervision. In *ECCV*.

Belharbi, S., Ben Ayed, I., McCaffrey, L., and Granger, E. (2019a). Deep ordinal classification with inequality constraints. *CoRR*, abs/1911.10720.

Belharbi, S., Rony, J., Dolz, J., Ben Ayed, I., McCaffrey, L., and Granger, E. (2019b). Min-max entropy for weakly supervised pointwise localization. *CoRR*, abs/1907.12934.

Beluch, W. H., Genewein, T., Nürnberger, A., and Köhler, J. M. (2018). The power of ensembles for active learning in image classification. In *CVPR*.

Bengio, Y., Delalleau, O., and Le Roux, N. (2010). Label propagation and quadratic criterion. In Chapelle, O., Scholkopf, B., and Zien, A., editors, *Semi-supervised learning*, chapter 11. The MIT Press.

Berlind, C. and Urner, R. (2015). Active nearest neighbors in changing environments. In *ICML*.

Bertsekas, D. (1999). Nonlinear programming, 2nd ed. chapter 4.

Casanova, A., Pinheiro, P., Rostamzadeh, N., and Pal, C. J. (2020). Reinforced active learning for image segmentation. In *ICLR*.

Dai, J., He, K., and Sun, J. (2015). Boxsup: Exploiting bounding boxes to supervise convolutional networks for semantic segmentation. In *ICCV*.

Deng, J., Dong, W., Socher, R., Li, L.-J., Li, K., and Fei-Fei, L. (2009). ImageNet: A Large-Scale Hierarchical Image Database. In *CVPR*.

Dolz, J., Desrosiers, C., and Ben Ayed, I. (2018). 3d fully convolutional networks for subcortical segmentation in mri: A large-scale study. *NeuroImage*, 170.

Ducoffe, M. and Precioso, F. (2015). Qbdc: query by dropout committee for training deep supervised architecture. *CoRR*, abs/1511.06412.

Ducoffe, M. and Precioso, F. (2018). Adversarial active learning for deep networks: a margin based approach. *CoRR*, abs/1802.09841.

Durand, T., Mordan, T., Thome, N., and Cord, M. (2017). Wildcat: Weakly supervised learning of deep convnets for image classification, pointwise localization and segmentation. In *CVPR*, volume 2.

Feige, U. (1998). A threshold of $\ln n$ for approximating set cover. *Journal of the ACM*, 45(4).

Fu, R., Hu, Q., Dong, X., Guo, Y., Gao, Y., and Li, B. (2020). Axiom-based grad-cam: Towards accurate visualization and explanation of cnns. *BMVC*.

Gal, Y., Islam, R., and Ghahramani, Z. (2017). Deep bayesian active learning with image data. In *ICML*.

Gaur, U., Kourakis, M., Newman-Smith, E., Smith, W., and Manjunath, B. (2016). Membrane segmentation via active learning with deep networks. In *ICIP*. IEEE.

Goodfellow, I., Bengio, Y., and Courville, A. (2016). *Deep Learning*. MIT Press. <http://www.deeplearningbook.org>.

Górriz Blanch, M. (2017). Active deep learning for medical imaging segmentation. B.S. thesis, Universitat Politècnica de Catalunya.

He, K., Zhang, X., Ren, S., and Sun, J. (2016). Deep residual learning for image recognition. In *CVPR*.

Huang, S.-J., Jin, R., and Zhou, Z.-H. (2010). Active learning by querying informative and representative examples. In *NIPS*.

Jia, Z., Huang, X., Chang, E. I.-C., and Xu, Y. (2017). Constrained deep weak supervision for histopathology image segmentation. *Transactions on medical imaging*, 36(11).

Kervadec, H., Dolz, J., Granger, E., and Ayed, I. B. (2019a). Curriculum semi-supervised segmentation. In *MICCAI*.

Kervadec, H., Dolz, J., Tang, M., Granger, E., Boykov, Y., and Ben Ayed, I. (2019b). Constrained-cnn losses for weakly supervised segmentation. *Medical image analysis*, 54.

Khoreva, A., Benenson, R., Hosang, J., Hein, M., and Schiele, B. (2017). Simple does it: Weakly supervised instance and semantic segmentation. In *CVPR*.

Kim, D., Cho, D., Yoo, D., and So Kweon, I. (2017). Two-phase learning for weakly supervised object localization. In *ICCV*.

Kim, K., Park, D., Kim, K. I., and Chun, S. Y. (2020). Task-aware variational adversarial active learning. *CoRR*, abs/2002.04709.

Kirsch, A., van Amersfoort, J., and Gal, Y. (2019). Batchbald: Efficient and diverse batch acquisition for deep bayesian active learning. In *NIPS*.

Kremer, J., Sha, F., and Igel, C. (2018). Robust active label correction. In *International Conference on Artificial Intelligence and Statistics*.

Krizhevsky, A., Sutskever, I., and Hinton, G. E. (2012). Imagenet classification with deep convolutional neural networks. In *NIPS*.

Lakshminarayanan, B., Pritzel, A., and Blundell, C. (2017). Simple and scalable predictive uncertainty estimation using deep ensembles. In *NIPS*.

Lin, D., Dai, J., Jia, J., He, K., and Sun, J. (2016). Scribblesup: Scribble-supervised convolutional networks for semantic segmentation. In *CVPR*.

Lin, M., Chen, Q., and Yan, S. (2013). Network in network. *coRR*, abs/1312.4400.

Litjens, G., Kooi, T., Bejnordi, B. E., Setio, A. A. A., and all (2017). A survey on deep learning in medical image analysis. *Medical Image Analysis*, 42.

Long, J., Shelhamer, E., and Darrell, T. (2015). Fully convolutional networks for semantic segmentation. In *CVPR*.

Long, J., Yin, J., Zhao, W., and Zhu, E. (2008). Graph-based active learning based on label propagation. In *International Conference on Modeling Decisions for Artificial Intelligence*.

Lubrano di Scandalea, M., Perone, C. S., Boudreau, M., and Cohen-Adad, J. (2019). Deep active learning for axon-myelin segmentation on histology data. *CoRR*, abs/1907.05143.

Malago, L., Cesa-Bianchi, N., and Renders, J. (2014). Online active learning with strong and weak annotators. In *NIPS Workshop on Learning from the Wisdom of Crowds*.

Mao, H. H. (2020). A survey on self-supervised pre-training for sequential transfer learning in neural networks. *CoRR*, abs/2007.00800.

Mattsson, B. (2017). Active learning of neural network from weak and strong oracles. Master's thesis.

Murugesan, K. and Carbonell, J. (2017). Active learning from peers. In *NIPS*.

Pathak, D., Krahenbuhl, P., and Darrell, T. (2015). Constrained convolutional neural networks for weakly supervised segmentation. In *ICCV*.

Pinheiro, P. H. O. and Collobert, R. (2015). From image-level to pixel-level labeling with convolutional networks. In *CVPR*.

Roels, J. and Saeys, Y. (2019). Cost-efficient segmentation of electron microscopy images using active learning. *CoRR*, abs/1911.05548.

Ronneberger, O., Fischer, P., and Brox, T. (2015). U-net: Convolutional networks for biomedical image segmentation. In *MICCAI*.

Rony, J., Belharbi, S., Dolz, J., Ben Ayed, I., McCaffrey, L., and Granger, E. (2019). Deep weakly-supervised learning methods for classification and localization in histology images: a survey. *CoRR*, abs/1909.03354.

Sener, O. and Savarese, S. (2018). Active learning for convolutional neural networks: A core-set approach. In *ICLR*.

Settles, B. (2009). Active learning literature survey. Technical report, University of Wisconsin-Madison Department of Computer Sciences.

Sinha, S., Ebrahimi, S., and Darrell, T. (2019). Variational adversarial active learning. In *ICCV*.

Sirinukunwattana, K., Pluim, J. P., Chen, H., et al. (2017). Gland segmentation in colon histology images: The glas challenge contest. *Medical image analysis*, 35.

Tang, M., Djelouah, A., Perazzi, F., Boykov, Y., and Schroers, C. (2018). Normalized Cut Loss for Weakly-supervised CNN Segmentation. In *CVPR*.

Teh, E. W., Rochan, M., and Wang, Y. (2016). Attention networks for weakly supervised object localization. In *BMVC*.

Tong, S. and Koller, D. (2001). Support vector machine active learning with applications to text classification. *JMLR*, 2.

Urner, R., David, S. B., and Shamir, O. (2012). Learning from weak teachers. In *Artificial intelligence and statistics*.

Vijayanarasimhan, S. and Grauman, K. (2012). Active frame selection for label propagation in videos. In *ECCV*.

Wah, C., Branson, S., Welinder, P., Perona, P., and Belongie, S. (2011). The Caltech-UCSD Birds-200-2011 Dataset. Technical report, California Institute of Technology.

Wang, K., Zhang, D., Li, Y., Zhang, R., and Lin, L. (2016). Cost-effective active learning for deep image classification. *IEEE Transactions on Circuits and Systems for Video Technology*, 27(12).

Wei, Y., Feng, J., Liang, X., Cheng, M.-M., Zhao, Y., and Yan, S. (2017). Object region mining with adversarial erasing: A simple classification to semantic segmentation approach. In *CVPR*.

Will, B., Le Petit, C., Berthelot, J., Tomiak, E., Verma, S., and Evans, W. (1999). Diagnostic and therapeutic approaches for nonmetastatic breast cancer in canada, and their associated costs. *British journal of cancer*, 79(9).

Yan, S., Chaudhuri, K., and Javidi, T. (2016). Active learning from imperfect labelers. In *NIPS*.

Yang, L., Zhang, Y., Chen, J., Zhang, S., and Chen, D. Z. (2017). Suggestive annotation: A deep active learning framework for biomedical image segmentation. In *MICCAI*.

Yoo, D. and Kweon, I. S. (2019). Learning loss for active learning. In *CVPR*.

Zhang, C. and Chaudhuri, K. (2015). Active learning from weak and strong labelers. In *NIPS*.

Zhou, D., Bousquet, O., Lal, T. N., Weston, J., and Schölkopf, B. (2004). Learning with local and global consistency. In *NIPS*.

Zhou, S., Chen, Q., and Wang, X. (2010). Active deep networks for semi-supervised sentiment classification. In *Proceedings of International Conference on Computational Linguistics: Posters*.

Zhou, Z.-H. (2017). A brief introduction to weakly supervised learning. *National Science Review*, 5.

Zhu, X. and Ghahramani, Z. (2002). Learning from labeled and unlabeled data with label propagation.

Zhu, X., Ghahramani, Z., and Lafferty, J. (2003). Semi-supervised learning using gaussian fields and harmonic functions. In *ICML*.